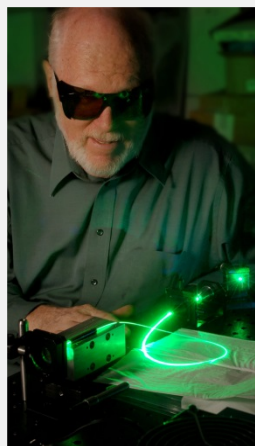
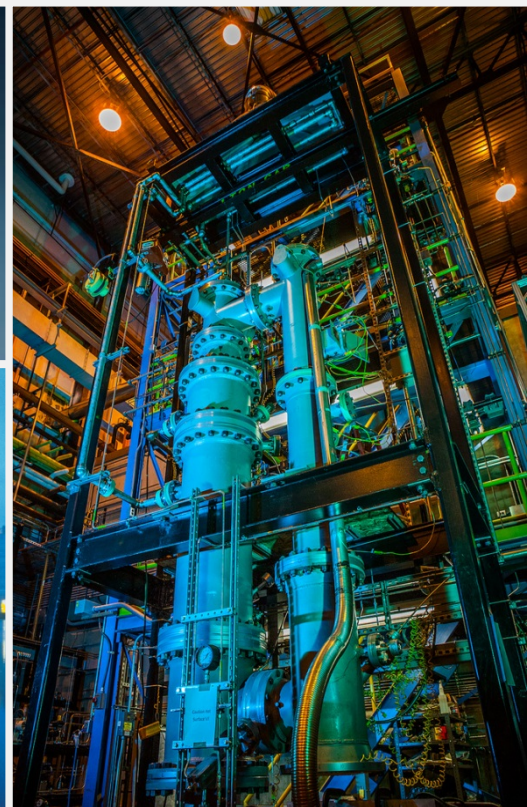
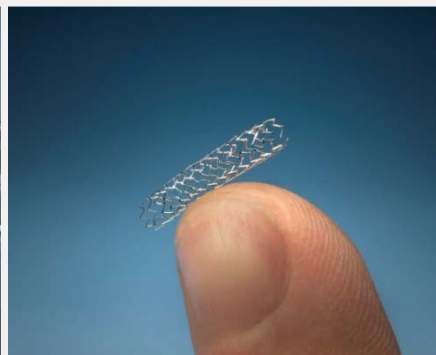
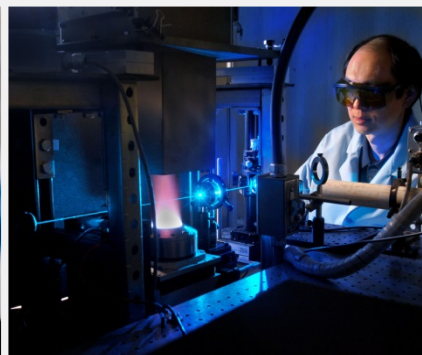




Driving Innovation ♦ Delivering Results



Materials Performance in Supercritical CO₂ in Comparison with Atmospheric CO₂ and Supercritical Steam

Gordon R Holcomb,
Ömer N. Doğan, Casey Carney,
Kyle Rozman, Jeffrey A. Hawk,
and Mark Anderson

The 5th International Symposium - Supercritical CO₂ Power Cycles
March 28-31, 2016, San Antonio, TX



U.S. DEPARTMENT OF
ENERGY

National Energy
Technology Laboratory

Acknowledgements



- **University of Wisconsin-Madison Collaboration**

- Arjun Kalra and Paul Brooks

- **Funding and Support**

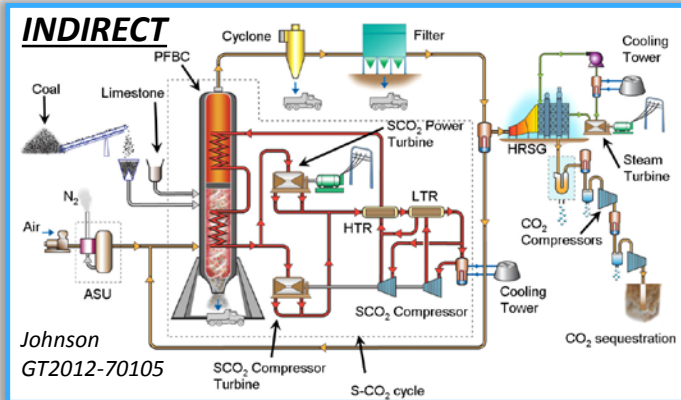
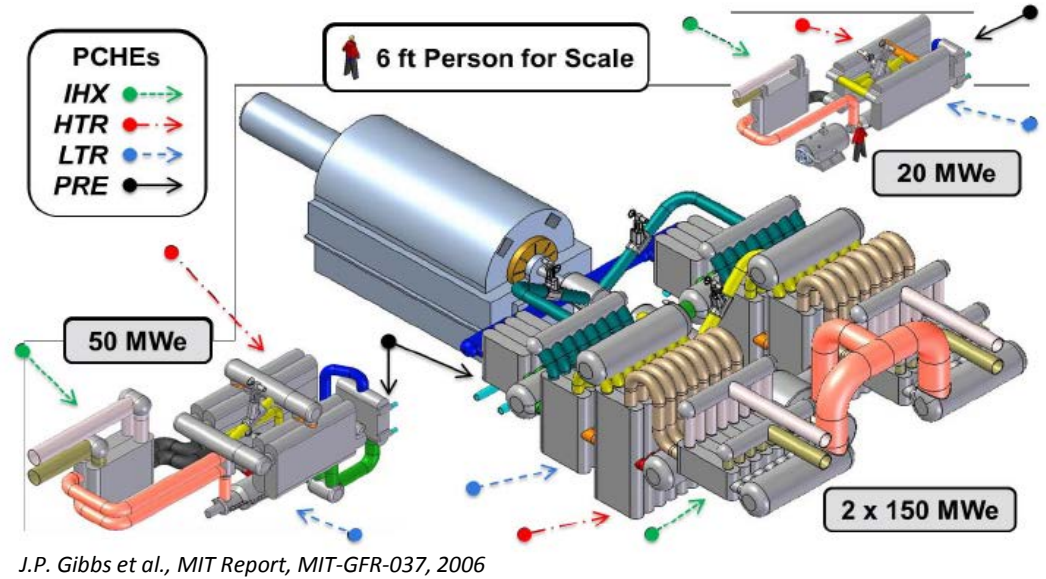
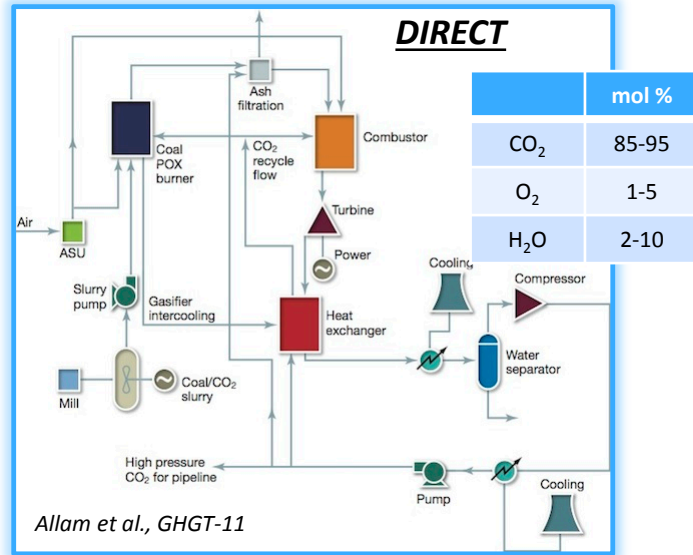
- This work was funded by the Advanced Combustion Program at the National Energy Technology Laboratory (Richard Dennis and Daniel Driscoll, Technology Managers and Briggs White, Project Monitor). The Research was executed through NETL's Research and Innovation Center's Advanced Combustion Field Work Proposal.

- **Disclaimer**

- "This report was prepared as an account of work sponsored by an agency of the United States Government. Neither the United States Government nor any agency thereof, nor any of their employees, makes any warranty, express or implied, or assumes any legal liability or responsibility for the accuracy, completeness, or usefulness of any information, apparatus, product, or process disclosed, or represents that its use would not infringe privately owned rights. Reference herein to any specific commercial product, process, or service by trade name, trademark, manufacturer, or otherwise does not necessarily constitute or imply its endorsement, recommendation, or favoring by the United States Government or any agency thereof. The views and opinions of authors expressed herein do not necessarily state or reflect those of the United States Government or any agency thereof."

- **Background**
 - Power cycles utilizing $s\text{CO}_2$
 - Comparison with steam system parameters
- **$s\text{CO}_2$, $s\text{H}_2\text{O}$, and $a\text{CO}_2$ Oxidation**
 - Experimental procedures
 - Results
 - Comparisons with other results
- **Summary/Conclusions**

sCO₂ Power Cycles



Cycle/Component	Inlet		Outlet		
	T (C)	P (bar)	T (C)	P (bar)	
Indirect	Heater	450-535	10-100	650-750	10-100
	Turbine	650-750	200-300	550-650	80-100
	HX	550-650	80-100	100-200	80-100
Direct	Combustor	750	200-300	1150	200-300
	Turbine	1150	200-300	800	30-80
	HX	800	30-80	100	30-80

Coal-based Steam Systems and Efficiency



Steam conditions and net plant efficiencies for pulverized coal power plants

Nomenclature	Conditions	Net Plant Efficiency (HHV)
Subcritical	2400 psi/1050°F/1050°F (165 bar/566°C/566°C)	35%
Supercritical (SC)	3600 psi/1050°F/1075°F 248 bar/566°C/579°C)	38%
Ultra-Supercritical (USC)	>3600 psi/1100°F/1150°F (>248 bar/593°C/621°C)	>42%
Advanced Ultra-Supercritical (A-USC)	4000-5000 psi/1300-1400°F (276-345 bar/704-760°C)	>45%

adapted from EPRI Report 1022770, 2011

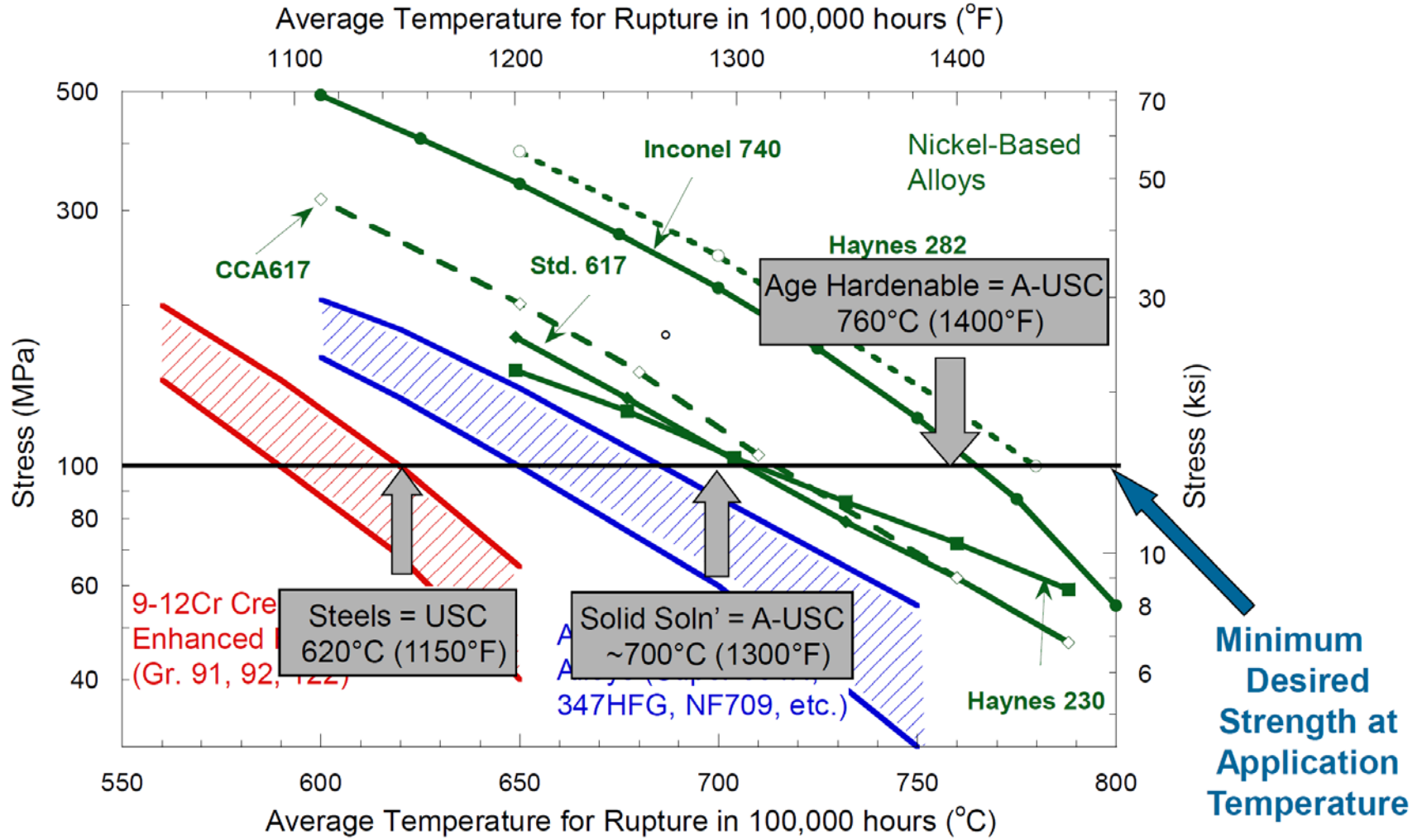
Categories are materials related, largely due to creep strength

- **USC: advanced ferritic & austenitic steels required**
- **A-USC: nickel-base superalloys required**

Each 1% increase in efficiency eliminates ~1,000,000 tons of CO₂ emissions over the lifetime of an 800-MW plant

Viswanathan, Armor, and Booras, 2003

Creep Rupture Advantages of Ni-Base Superalloys



Shingledecker, Purgert, and Cedro, 2013

sCO2 Components/A-USC Conditions



Nomenclature	Conditions
Subcritical	2400 psi/1050°F/1050°F (165 bar/566°C/566°C)
Supercritical (SC)	3600 psi/1050°F/1075°F 248 bar/566°C/579°C)
Ultra-Supercritical (USC)	>3600 psi/1100°F/1150°F (>248 bar/593°C/621°C)
Advanced Ultra-Supercritical (A-USC)	4000-5000 psi/1300-1400°F (276-345 bar/704-760°C)

adapted from EPRI Report 1022770, 2011

Similarities in temperature and pressure suggests similar alloy candidates

Cycle/Component		Inlet		Outlet	
		T (C)	P (bar)	T (C)	P (bar)
Indirect	Heater	450-535	10-100	650-750	10-100
	Turbine	650-750	200-300	550-650	80-100
	HX	550-650	80-100	100-200	80-100
Direct	Combustor	750	200-300	1150	200-300
	Turbine	1150	200-300	800	30-80
	HX	800	30-80	100	30-80

Alloys and Samples



Alloy	Fe	Cr	Ni	Co	Mo	Si	Ti	Al	Mn	Cu	V	Nb	C
347H	Bal	17.6	9.1	0.1	0.2	0.3			1.1	0.1	0.1	0.7	0.05
282	0.2	19.4	Bal	10.1	8.7		2.2	1.4					0.06
625	3.4	22.1	Bal		8.9	0.1	0.2	0.1	0.1	0.2		3.3	0.05



Compact Tension Specimens
Nominally 22 × 23 × 3 mm

Ground surfaces to 600 grit

Triplicate Specimens in each test

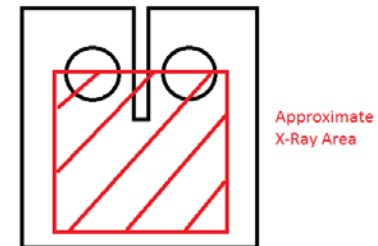
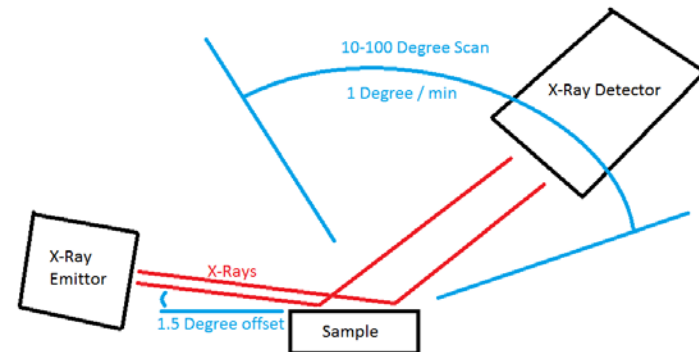
Experimental Conditions for 500 h Tests



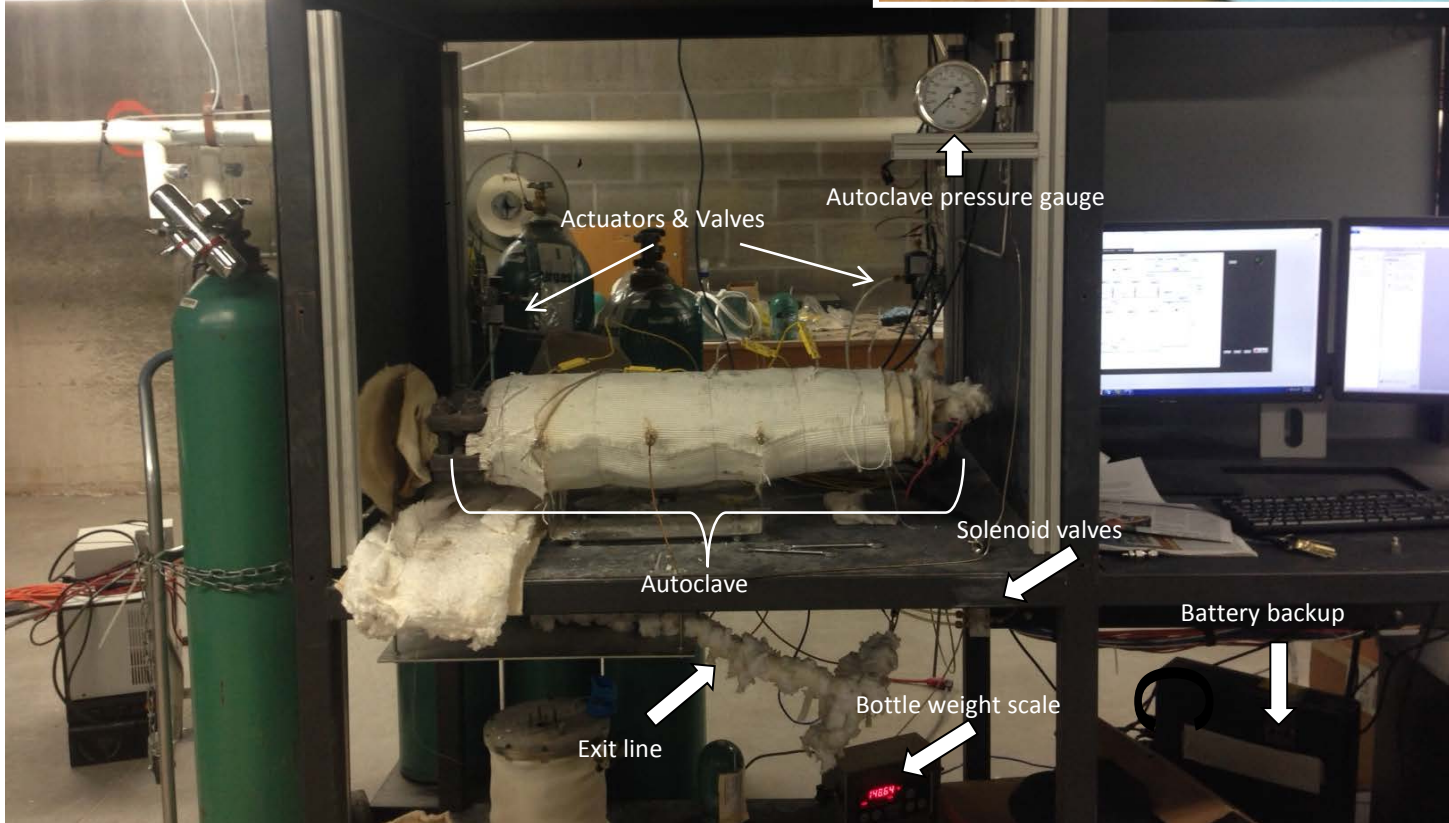
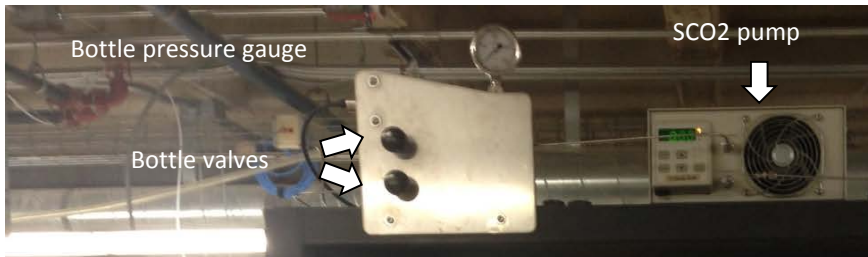
Test	T, °C	P, bar	Environment	ρ , g/cm ³	u, cm/min	Re
sCO ₂	730	207	99.999% CO ₂	1.04×10^{-1}	0.40	10.4
sH ₂ O	726	208	Deaerated H ₂ O	4.77×10^{-2}	0.21	1.8
aCO ₂	730	1	CO ₂ with 0.25% O ₂	5.28×10^{-4}	33.0	4.8

Results

- Mass change
- Surface SEM
- Glancing angle (1.5°) XRD
- Cross-section SEM



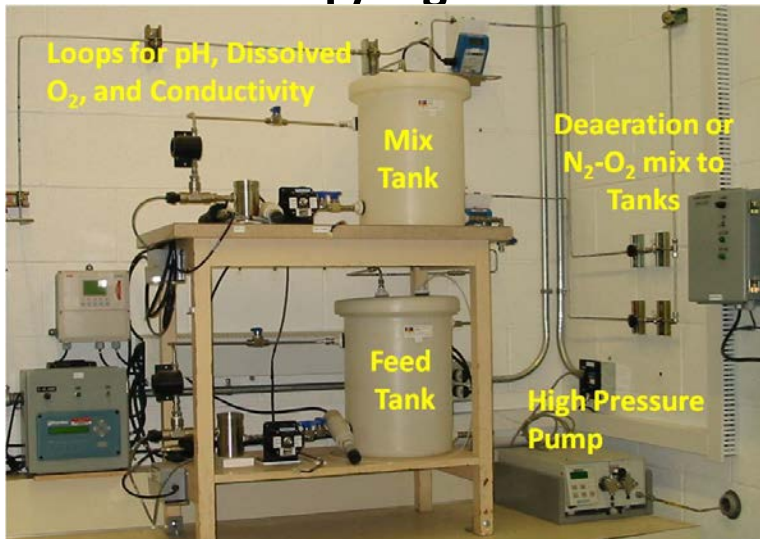
System for sCO₂ Exposures



USC Autoclave for sH2O Exposures



Feed Water Prep/High Pressure Pump



Flow Rate
Controlled by
Pump

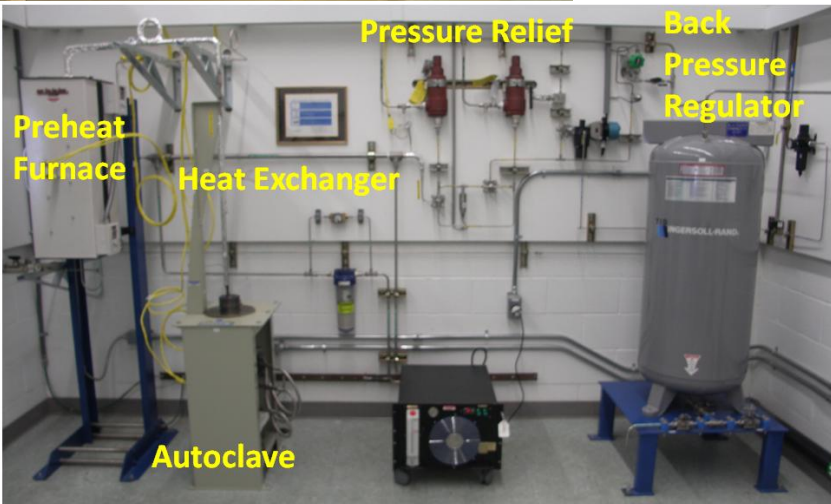
Pressure
Controlled by
Back Pressure
Regulator



Autoclave

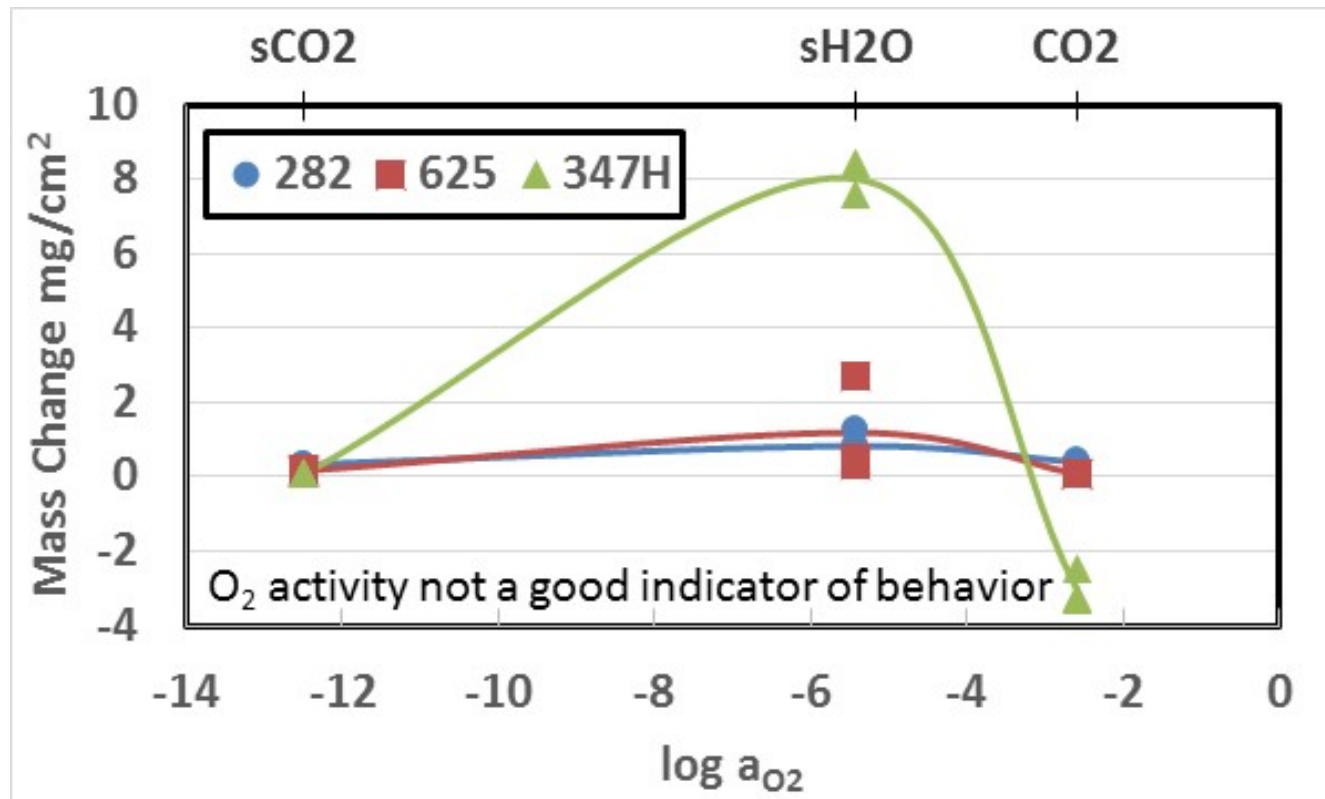


High
Pressure
Side



Autoclave
1 Liter
6.35 cm ID
31.75 cm L

Mass Change Results



Mass Change, mg/cm²

Test	282	625	347H
sCO ₂	0.36	0.16	0.10
	0.33	0.15	0.08
	0.33	0.21	0.08
sH ₂ O	0.87	2.73	8.44
	1.25	0.53	7.58
	0.39	0.31	0.79*
CO ₂	0.40	0.09	-2.47
	0.42	0.08	-3.33
	0.37	0.07	-3.23

*SEM revealed significant spalling, so not used in plots or k_p calculations

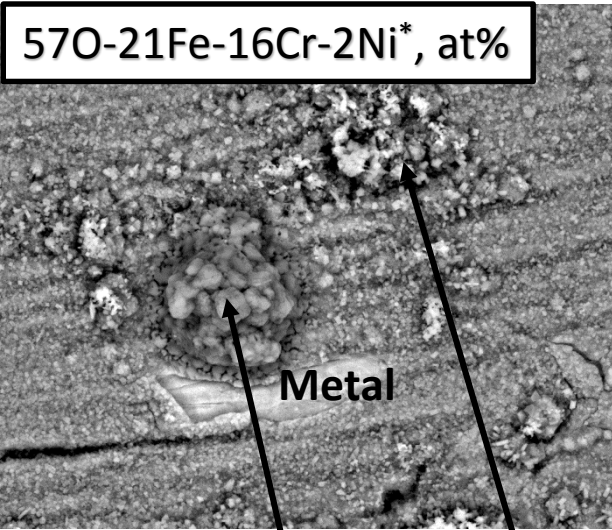
Surface SEM – 347H



Alloy	Fe	Cr	Ni	Co	Mo	Si	Ti	Al	Mn	Cu	V	Nb	C
347H	Bal	17.6	9.1	0.1	0.2	0.3			1.1	0.1	0.1	0.7	0.05

sCO₂ +0.08 mg/cm²

57O-21Fe-16Cr-2Ni*, at%



Metal

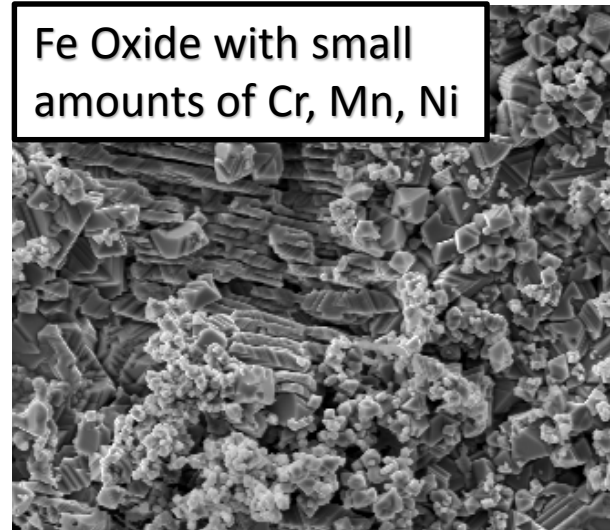
20 μm

Nb-Rich & Low Cr

Mn-Rich & Low Cr

sH₂O +7.62 mg/cm²

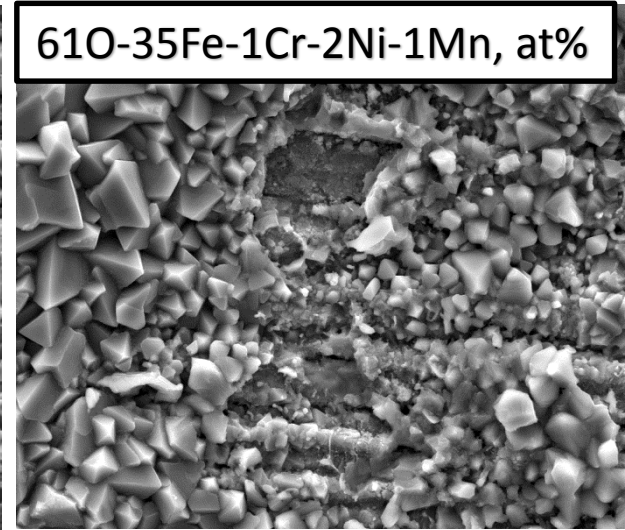
Fe Oxide with small amounts of Cr, Mn, Ni



20 μm

CO₂ -3.33 mg/cm²

61O-35Fe-1Cr-2Ni-1Mn, at%



20 μm

Chromia with nodule formation of Low Cr oxides
Scale spalling tendencies

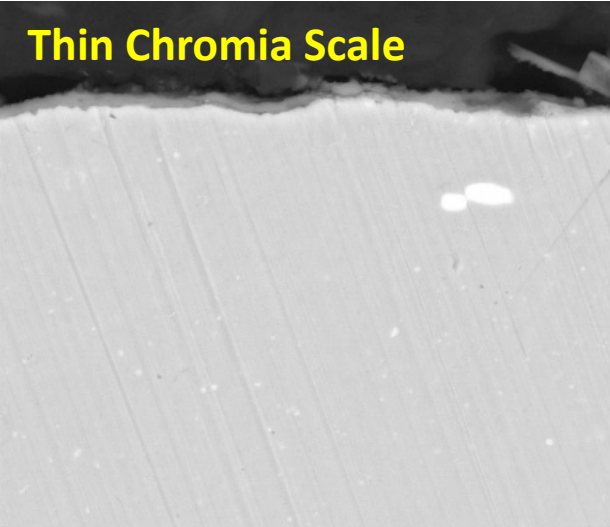
*Glancing angle XRD confirms Cr₂O₃ and M₃O₄ as the primary surface phases

Cross-section SEM – 347H



Alloy	Fe	Cr	Ni	Co	Mo	Si	Ti	Al	Mn	Cu	V	Nb	C
347H	Bal	17.6	9.1	0.1	0.2	0.3			1.1	0.1	0.1	0.7	0.05

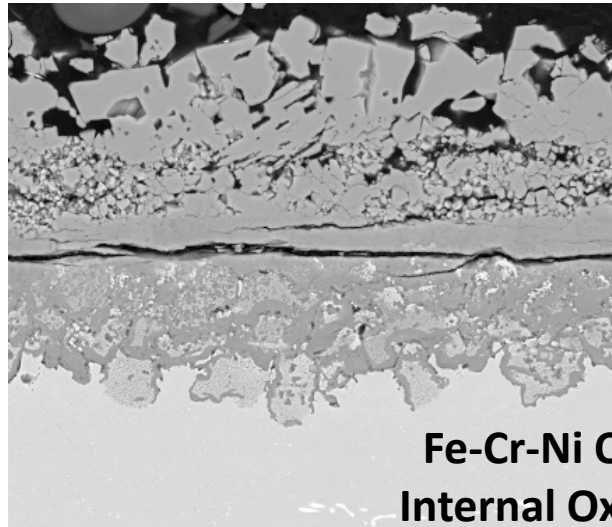
sCO₂ +0.10 mg/cm²



Thin Chromia Scale

10 μm

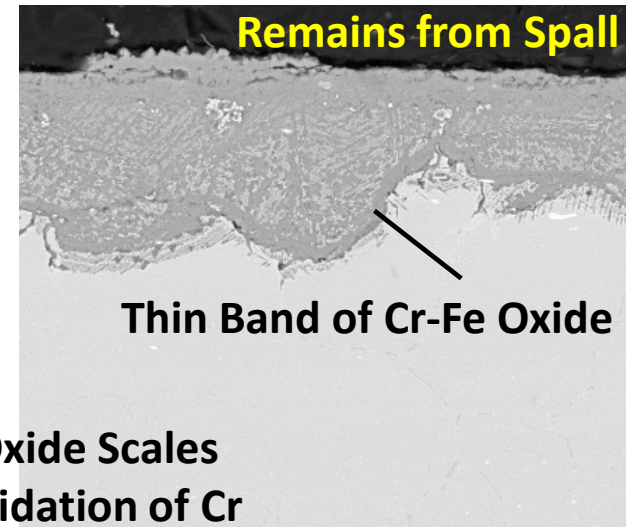
sH₂O +8.44 mg/cm²



**Fe-Cr-Ni Oxide Scales
Internal Oxidation of Cr**

50 μm

aCO₂ -2.47 mg/cm²



Remains from Spall

Thin Band of Cr-Fe Oxide

50 μm

- Protective oxide in sCO₂
- Less protective oxides in sH₂O and aCO₂
- Will show later that this switch from protective oxidation is typical

Surface SEM - 282



Alloy	Fe	Cr	Ni	Co	Mo	Si	Ti	Al	Mn	Cu	V	Nb	C
282	0.2	19.4	Bal	10.1	8.7		2.2	1.4					0.06

sCO₂ +0.33 mg/cm²

62O-31Cr-7Ti-1Ni*, at%

70O-26Cr-2Ti-3Ni, at%

sH₂O +1.25 mg/cm²

65O-24Cr-6Ni-3Ti-1Co*, at%

aCO₂ +0.42 mg/cm²

62O-30Cr-7Ti-1Ni*, at%

10 μm

10 μm

10 μm

Chromia scale with TiO₂ on outer surface

*Glancing angle XRD confirms Cr₂O₃ and TiO₂ as the primary surface phases

Cross-section SEM - 282

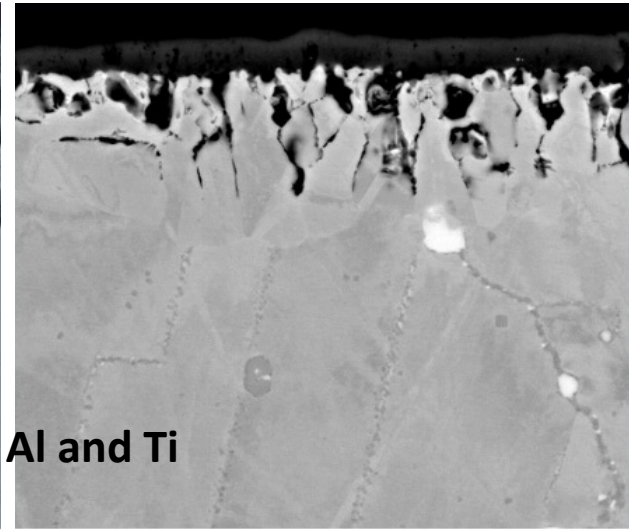
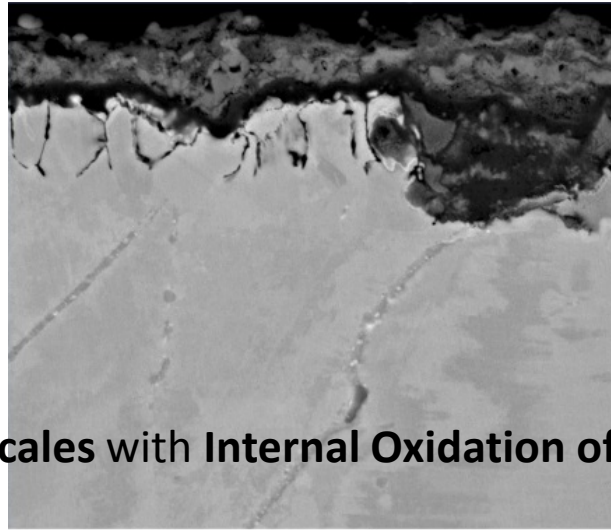
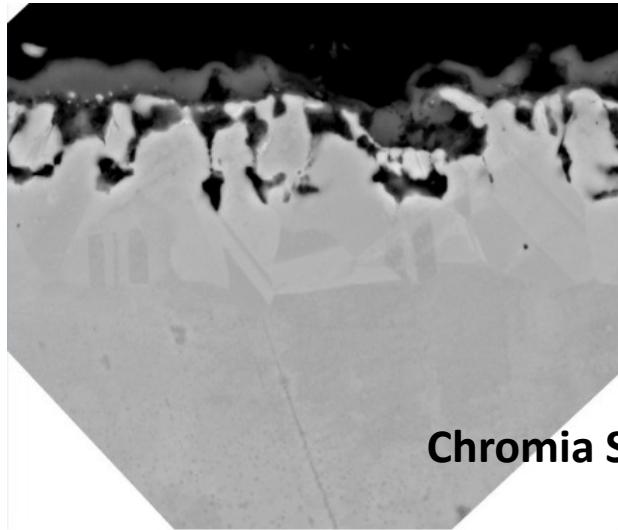


Alloy	Fe	Cr	Ni	Co	Mo	Si	Ti	Al	Mn	Cu	V	Nb	C
282	0.2	19.4	Bal	10.1	8.7		2.2	1.4					0.06

$s\text{CO}_2$ +0.36 mg/cm²

$s\text{H}_2\text{O}$ +0.87 mg/cm²

$a\text{CO}_2$ +0.40 mg/cm²



Chromia Scales with Internal Oxidation of Al and Ti

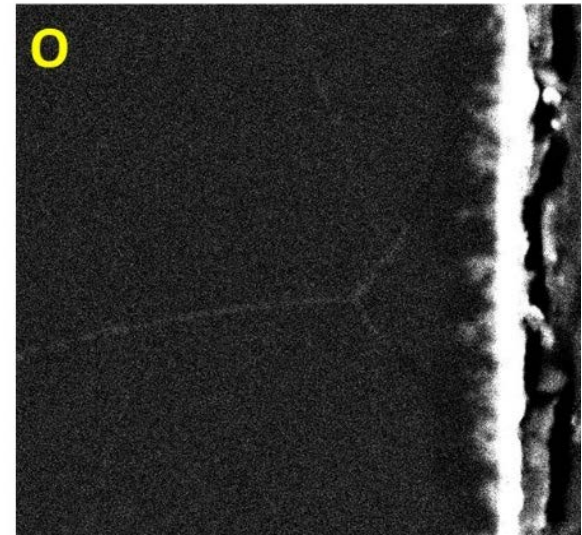
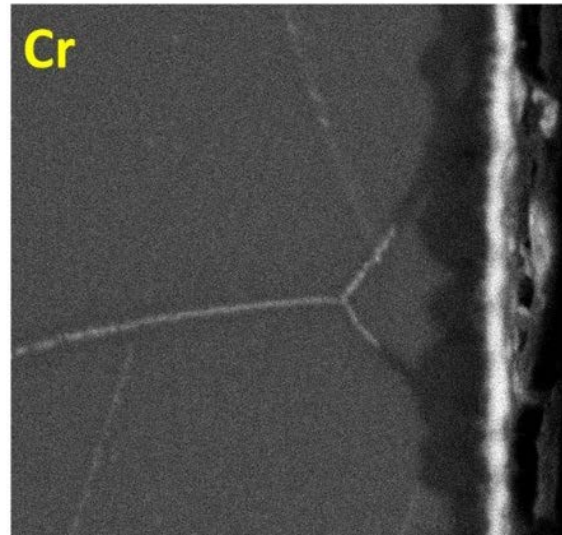
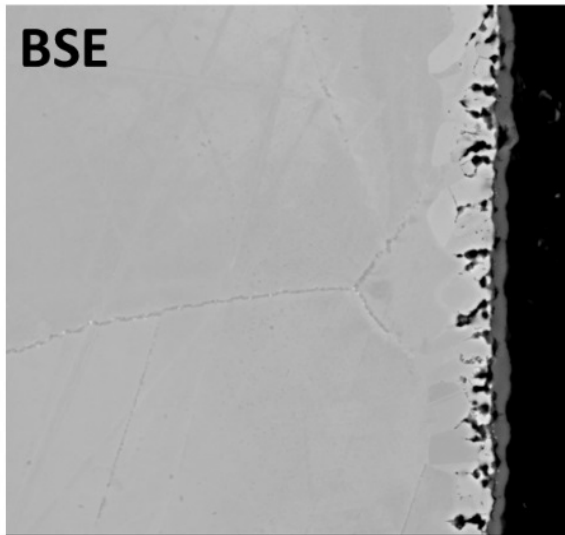
10 μm

10 μm

10 μm

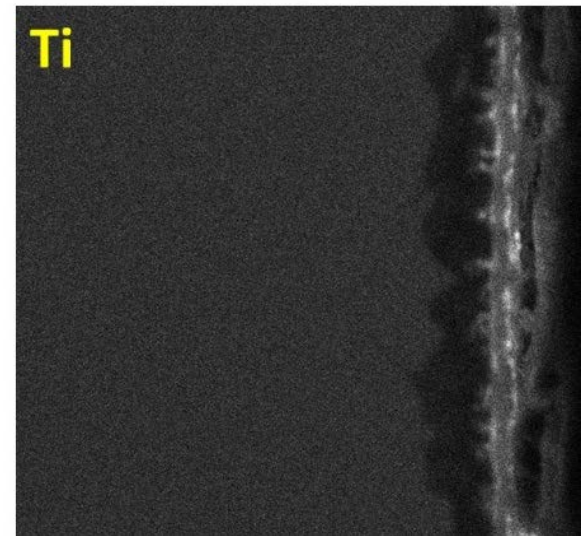
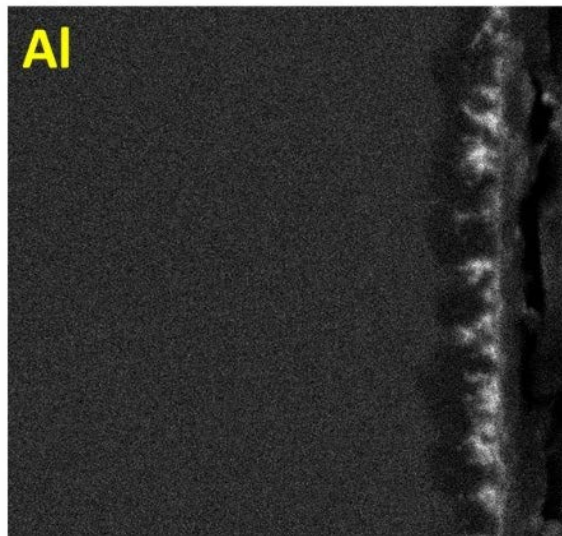
- Protective chromia scale thicker in $s\text{H}_2\text{O}$
- Internal oxidation deeper and more extensive in CO_2

EDS Mapping of 282 in sCO₂



30 μm

- Depletion of Cr, Al, Ti below internal oxidation zone
- Loss of γ' and strength



Surface SEM - 625



Alloy	Fe	Cr	Ni	Co	Mo	Si	Ti	Al	Mn	Cu	V	Nb	C
625	3.4	22.1	Bal		8.9	0.1	0.2	0.1	0.1	0.2		3.3	0.05

sCO₂ +0.15 mg/cm²

70O-20Cr-7Ni-1Mo-1Nb*, at%

sH₂O +0.53 mg/cm²

63O-17Cr-15Ni-2Mo-1Fe*, at%

aCO₂ +0.08 mg/cm²

68O-17Cr-11Ni-2Mo-1Nb*, at%

10 μm

10 μm

10 μm

Chromia scale with some underlying alloy Ni content showing in analysis

71O-28Cr-1Ni-1Nb, at%

*Glancing angle XRD confirms Cr₂O₃ as the primary surface phase

Cross-section SEM - 625



Alloy	Fe	Cr	Ni	Co	Mo	Si	Ti	Al	Mn	Cu	V	Nb	C
625	3.4	22.1	Bal		8.9	0.1	0.2	0.1	0.1	0.2		3.3	0.05

sCO₂ +0.16 mg/cm²

sH₂O +2.73 mg/cm²

aCO₂ +0.09 mg/cm²

Chromia Scale

Ni-Cr-Mo-Fe Oxide Scale

Chromia Scale

Some areas in aCO₂
had thicker scales

10 μm

100 μm

10 μm

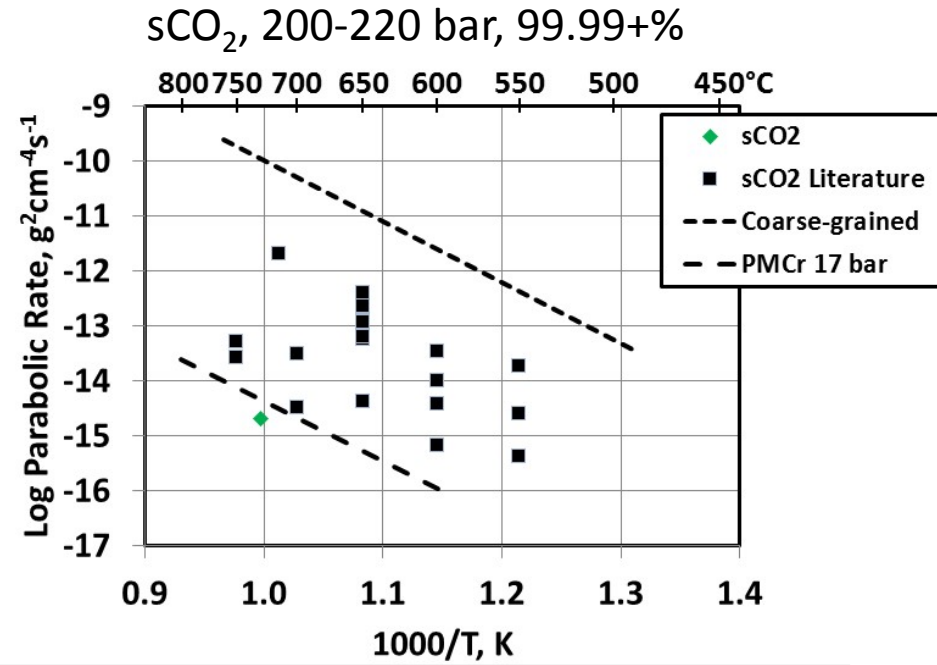
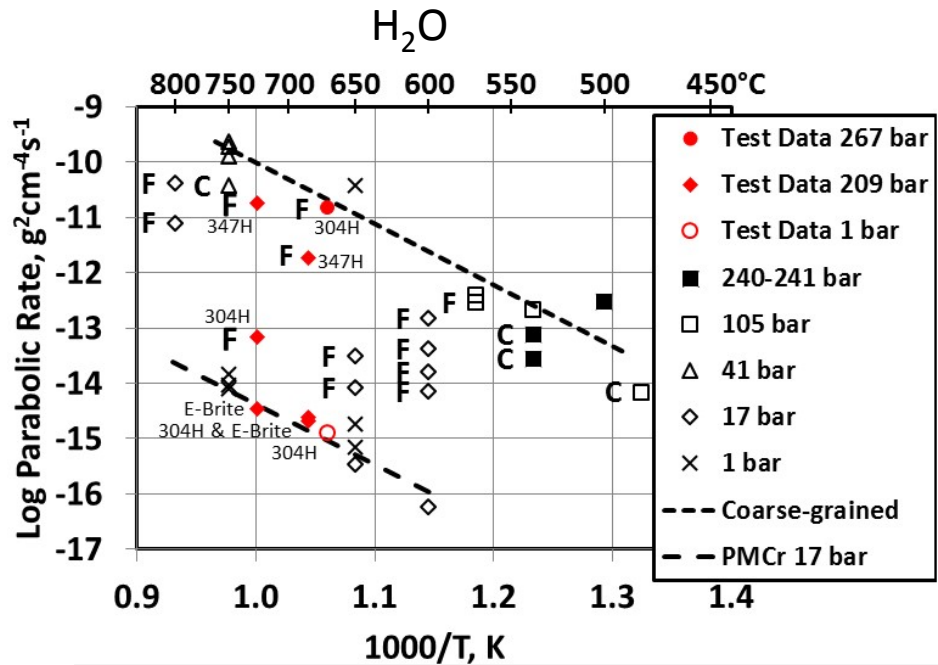
- Other 2 replicates in sH₂O had much smaller mass gains and chromia was detected on the surface by XRD
- Bright second phases are Nb/Mo rich

- **Parabolic rate constants were estimated using**

$$k_p = \frac{\Delta M^2}{2t}$$

- Where ΔM is the mass change and t is the time
- **Time series tests are planned to verify such behavior**
- **Not applied in cases where spalling was evident**

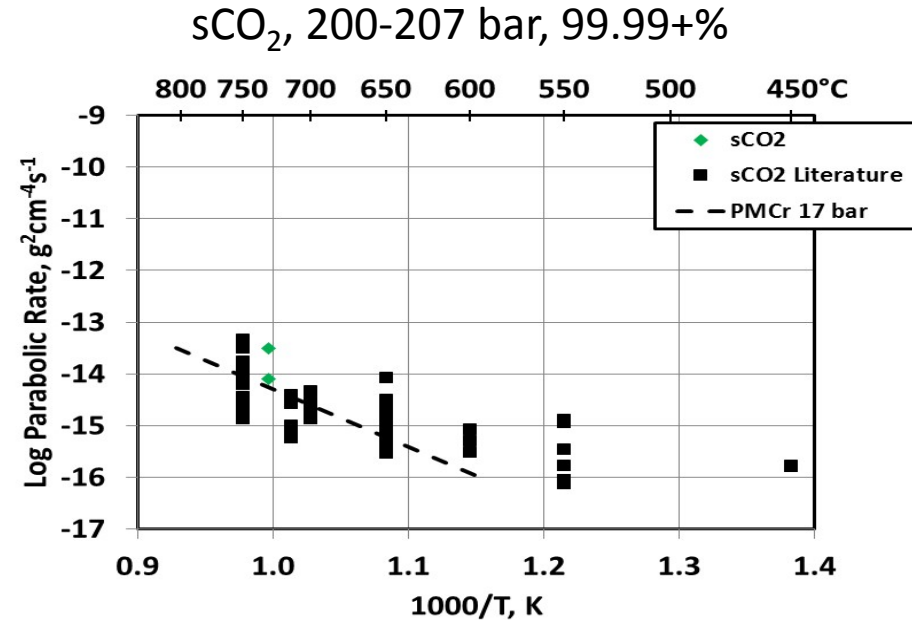
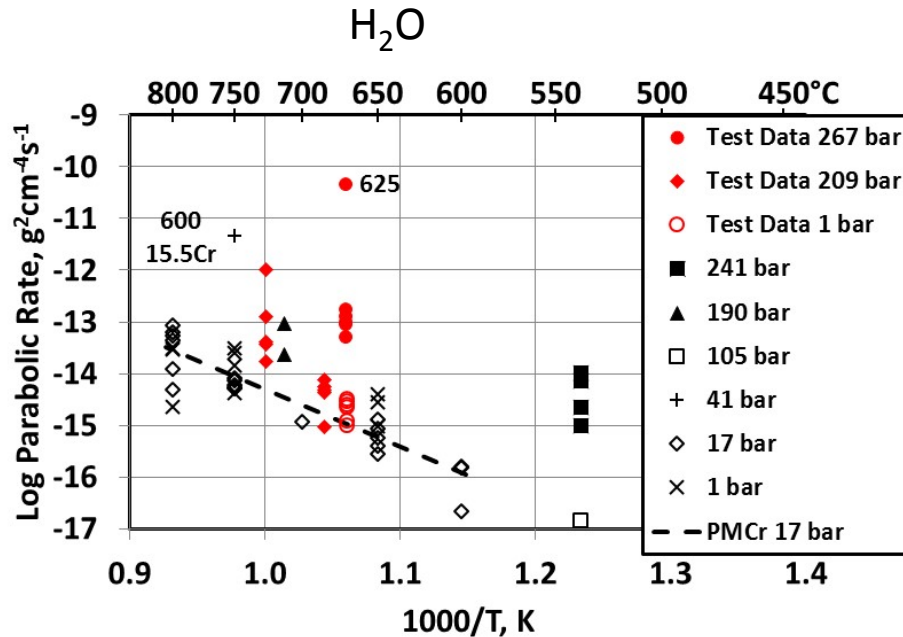
300 Series (18Cr-8Ni)/E-Brite



- Similar behavior in both $s\text{H}_2\text{O}$ and $s\text{CO}_2$ (but note the gap in $s\text{CO}_2$)
- A variable increase in oxidation of fine-grain alloys with pressure
- Variability arises from Fe-rich nodule formation and lateral growth to disrupt protective chromia scale

H_2O adapted from the compilation of Wright & Dooley (2010), plus Holcomb (2014) and Holcomb (2016)
 $s\text{CO}_2$ adapted from Furukawa (2011), Cao (2012), Pint (2014), Lim (2008), Olivares (2015), Dunlevy (2007), and Lee (2015)

Ni-base Alloys

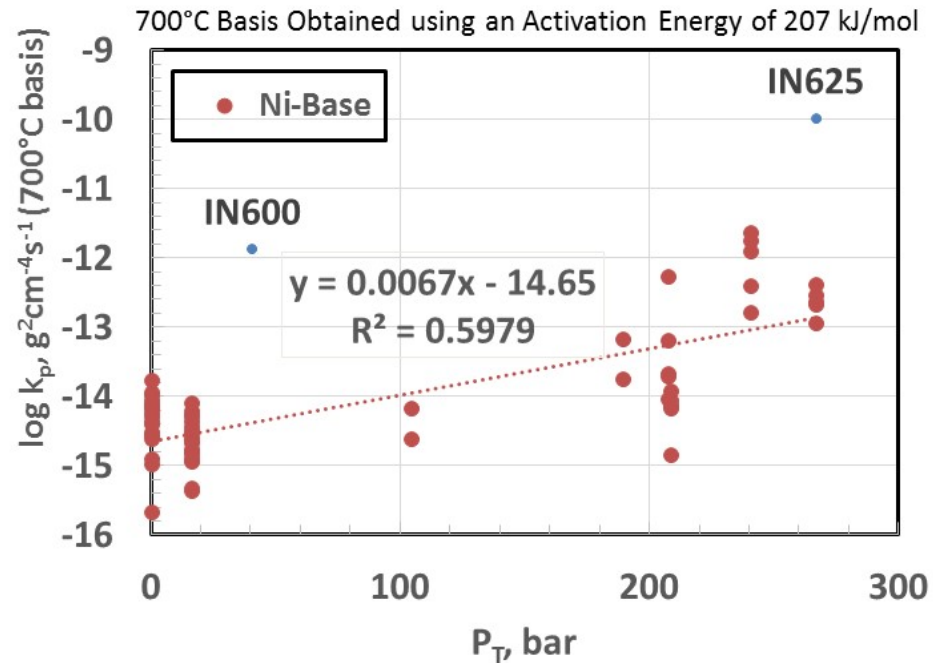
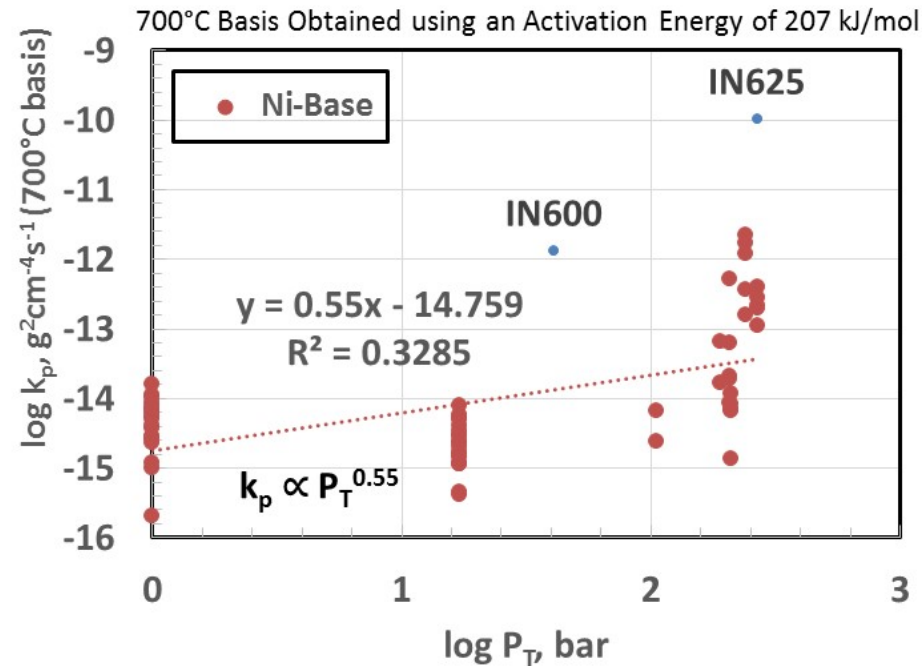


- The highest pressures in sH₂O show an increased oxidation rate
- No evidence of increased oxidation rates at high pressure in sCO₂ (at temperatures of interest)
- 625 has ~8000 h in a steam superheater at ~713°C/190 bar with good performance Knödler (2014)

H₂O adapted from the compilation of Wright & Dooley (2010), plus Knödler (2014), Holcomb (2014) and Holcomb (2016)

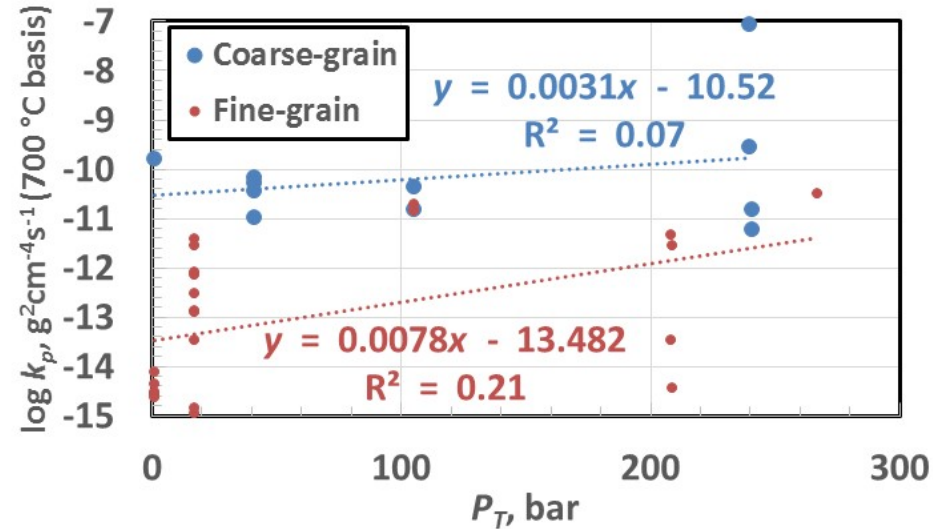
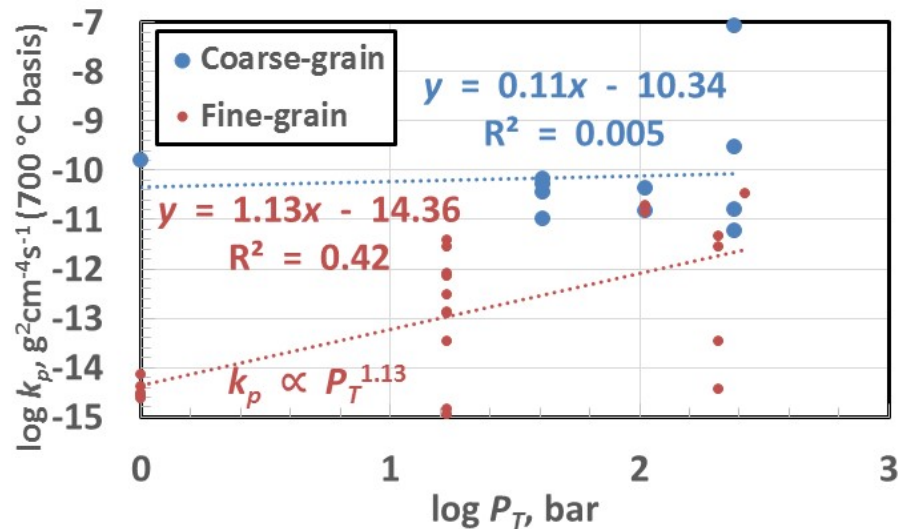
sCO₂ adapted from Pint (2014), Dunlevy (2007), Lee (2014, 2015), Firouzdar (2013), Dheeradhada (2015), and Mahaffey (2015)

Effect of Pressure in Steam for Ni Alloys



- Arrhenius behavior used to translate oxidation data to a 700°C basis
- Oxide defect models tend to predict $k_p \propto P_T^X$
- Better fit with $\log k_p \propto P_T$

Effect of Pressure in Steam for Austenitics



- Arrhenius behavior used to translate oxidation data to a 700°C basis
- Oxide defect models tend to predict $k_p \propto P_T^x$
- Fine Grain Alloys: Better fit with $\log k_p \propto \log P_T$ ($k_p \propto P_T^{1.13}$)
- Coarse Grain Alloys: No measurable dependence on pressure

- **High Pressure sH₂O and sCO₂ Exposures**
 - Over 200 bar and 726-730°C
- **Preliminarily Results Indicate:**
 - Nickel-base alloys
 - Unlike in sH₂O, there is no evidence of significant increased oxidation rates at high pressure in sCO₂
 - Fine-grain austenitic steels
 - Similar increase in oxidation with pressure in both sH₂O and sCO₂
 - More Fe-rich oxide nodule formation with pressure
 - Variability in results associated with nodule formation/lateral growth
 - Coarse-grain austenitic steels
 - No measurable increase in oxidation with pressure in sH₂O
 - Not examined in sCO₂